

01,11,10

Diffusion along asymmetrical grain boundary with misorientation axis [110]

© A.V. Weckman, B.F. Dem'yanov

Polzunov Altai State Technical University,
Barnaul, Russia

E-mail: weckman@list.ru

Received April 26, 2024

Revised April 26, 2024

Accepted April 27, 2024

The study of grain boundary self-diffusion along asymmetric grain boundaries with the axis of misorientation [110] was carried out using computer modeling methods. The misorientation angle of asymmetric boundaries corresponds to the misorientation angle of the special grain boundary $\Sigma 11(113)$. The calculation was carried out using of the Morse pair potential and the Cleri–Rosato many-body potential. It is shown that the structure of asymmetrical grain boundaries can be described in the model of structural units — all grain boundaries contain structural elements specific of the $\Sigma 11(113)$ boundary. The coefficients of grain boundary diffusion were calculated and Arrhenius dependencies were constructed, according to which the activation energies of diffusion were determined. Dependencies have from two to four linear sections. It was found that at high temperatures the grain boundary region amorphized earlier than adjacent grains. This suggests that the boundaries melt at lower temperatures, which ranged from 0.91 to 0.98 melting temperatures.

Keywords: Grain boundary, computer simulation, grain boundary diffusion, melting of grain boundary.

DOI: 10.61011/PSS.2024.05.58619.105

1. Introduction

It is well known that the rate of grain-boundary (GB) diffusion is much higher than the corresponding rate inside the grain [1]. This high rate of GB diffusion is due to a significant excess free volume and an elevated energy of atoms near the boundary. A considerable amount of literature has been published on diffusion. However, most studies are focused on well-examined special boundaries with a low index of reciprocal density of coincident sites Σ . It should be noted that the experimental study of diffusion is hindered by the fact that interpretation of experimental data is sometimes ambiguous due to inhomogeneity of boundary structure and failure to achieve strict qualification of boundaries. Computer-based simulation of diffusion processes is used to investigate GB having precise values of misorientation axis and angle, boundary depth plane and other parameters. Moreover, the computer-based experiment detects the effects that cannot be measured by experimental methods. Thus, the investigation of diffusion on GBs with low Σ values [2] showed that diffusion movement depends on the boundary structure and the Arrhenius dependences have a linear form for all boundaries and all directions. However, near the melting temperature [3] diffusion becomes almost independent on the boundary structure and the Arrhenius dependence changes its inclination. The same result was reported by the authors of [4,5] who investigated special tilt $\Sigma 5$ boundaries with misorientation axis [100]. Several linear segments in the temperature dependence were found in [6] in the study of symmetrical tilt grain boundaries in intermetallic Ni_3Al .

In other studies, for example, in [7], the Arrhenius dependences have a linear behavior throughout the temperature range, and the activation energy and pre-exponential factor of diffusion constant are highly anisotropic and depend on the GB misorientation angle. A similar result was obtained in [8] in the investigation of special $\Sigma 5(012)$ and $\Sigma 5(013)$ boundaries. The authors of [9] pointed out the anisotropy of hydrogen diffusion on special $\Sigma 19$ GBs in BCC Fe. This anisotropy is attributable to the boundary structure.

Diffusion on asymmetrical grain boundaries was investigated in [10]. A special $\Sigma 5(013)$ GB in Ni and a series of asymmetrical boundaries with the same misorientation angle were chosen as the objects of study. It is shown that the self-diffusion coefficient is highly dependent on the boundary depth plane at low temperature, but almost does not depend on high temperature. Diffusion activation energy on a symmetrical boundary is much higher than on an asymmetrical boundary.

2. Structure of asymmetrical grain boundaries

The present study is focused on diffusion on asymmetric grain boundaries in aluminum with misorientation angle $\Theta = 50.48^\circ$ in the $0.45T_m < T < T_m$ temperature range, where T_m is the melting temperature. This angle was chosen for the fact that it is the misorientation angle of symmetric tilt boundary $\Sigma 11(113)$ with misorientation axis [110], which is highlighted in the energy curves [11–13]. Figure 1

Table 1. Crystallographic parameters of GBs: reciprocal density of coincident sites (Σ), boundary plane (hkl), and misorientation angles of asymmetrical boundaries (Θ_1 , Θ_2)

Σ	hkl	$\Theta_1, ^\circ$	$\Theta_2, ^\circ$
51	1110	8.0494	42.4293
33	118	10.0249	40.4538
19	116	13.2627	37.2161
27	115	15.7932	34.6856
9	114	19.4712	31.0076
11	113	25.2394	25.2394
41	338	27.9384	22.5405
33	225	29.4962	20.9826
3	112	35.2644	15.2144
17	223	43.3139	7.1649
17	334	46.6861	3.7927

presents the diagram of construction of the studied asymmetrical boundaries. The axes of the laboratory coordinate frame were positioned as follows: axis Ox coincides with the boundary misorientation axis; axis Oy goes along the boundary plane perpendicular to the misorientation axis; and axis Oz is perpendicular to the GB plane. These boundaries are formed by rotating the upper crystal by angles Θ_1 that correspond to special grain boundaries, and Θ_2 is such that the sum of these two angles yields a value of $\Theta = 50.48^\circ$. Angles Θ_1 are equal to half the misorientation angles of symmetrical grain boundaries, which are special GBs with reciprocal density of coincident sites Σ in the CSL model. The values of Σ and the corresponding angles Θ_1 are listed in Table 1. Table 1 also presents the values of angles Θ_2 and Miller indices (hkl) of the boundary plane relative to the upper crystal, which will be used to identify the boundaries.

A simple geometric procedure (the same as in the CSL model) was used as the initial configuration of atoms near the boundary; i.e., two halves of the bicrystal are rotated about an axis passing through one of the atomic rows. The rotation angle of one of the interfacing crystal blocks does not depend on the other.

The Morse pair potential [14] and the Cleri–Rosato many-body potential [15] were used in calculations. The Morse potential parameters were taken from [16], and the Cleri–Rosato parameters were taken from [15]. Comparison of data calculated using two different potentials has shown that the GB structure does not depend on the selected form of potential [17]. Simple geometrical configuration of the boundary assumes that some atoms in the GB region are at a distance that differs from the equilibrium distance and as a result the boundary has high energy value. Introduction of additional atoms and vacancies stabilizes the boundary structure and considerably decreases its energy [18]. This procedure is known as a vacancy relaxation [19–20]. The vacancy relaxation is followed by atomic displacement under the action of interatomic forces that additionally decreases the GB energy and stabilizes its structure.

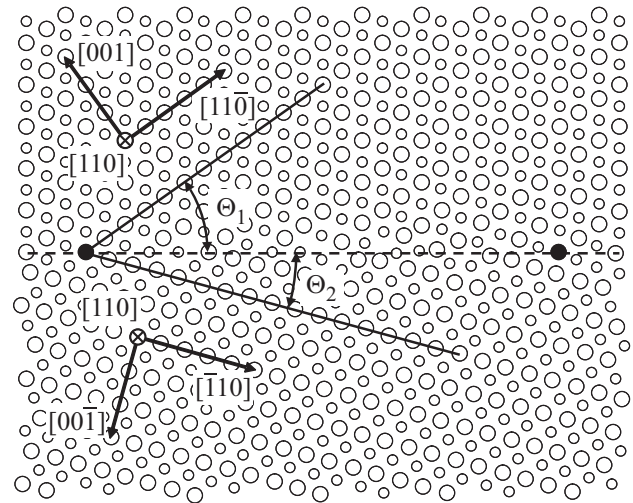


Figure 1. Construction of asymmetrical grain boundaries.

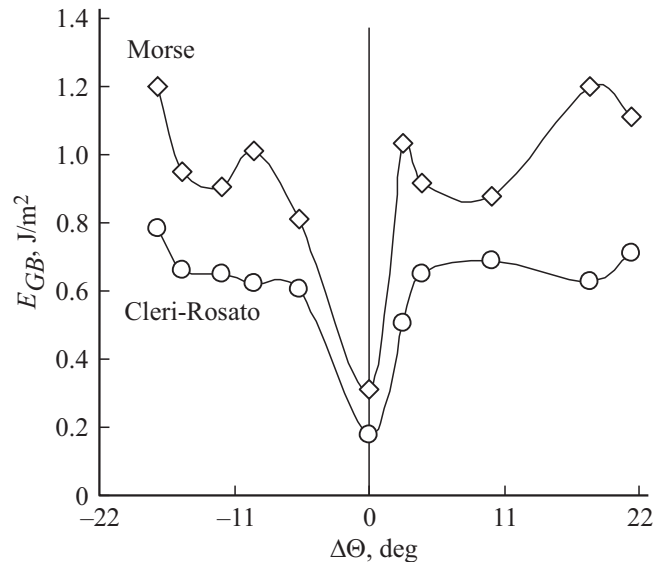


Figure 2. Energy of asymmetrical grain boundaries.

For ease of comparison of energies of the studied GBs, Figure 2 presents the dependence of the GB energy on parameter $\Delta\Theta = \Theta_1 - \Theta_2/2$. The value of $\Delta\Theta = 0$ corresponds to symmetrical boundary $\Sigma 11(113)$, and the rest are asymmetrical GBs. It is evident that GB $\Sigma 11(113)$, which is a special boundary, has a much lower energy than asymmetrical boundaries when both the pair potential and the many-body potential are used.

It was demonstrated in [17,21] that symmetrical boundary $\Sigma 11(113)$ consists of strictly alternating similar structural elements. The study of structure of asymmetrical boundaries revealed that they all contain the same structural elements (Figure 3), which are deformed and rotated relative to the boundary plane; notably, the greater the difference between Θ_1 and Θ_2 , the more deformed these elements are. The distance between elements varies from the minimum one to several lattice parameters. The structures of some

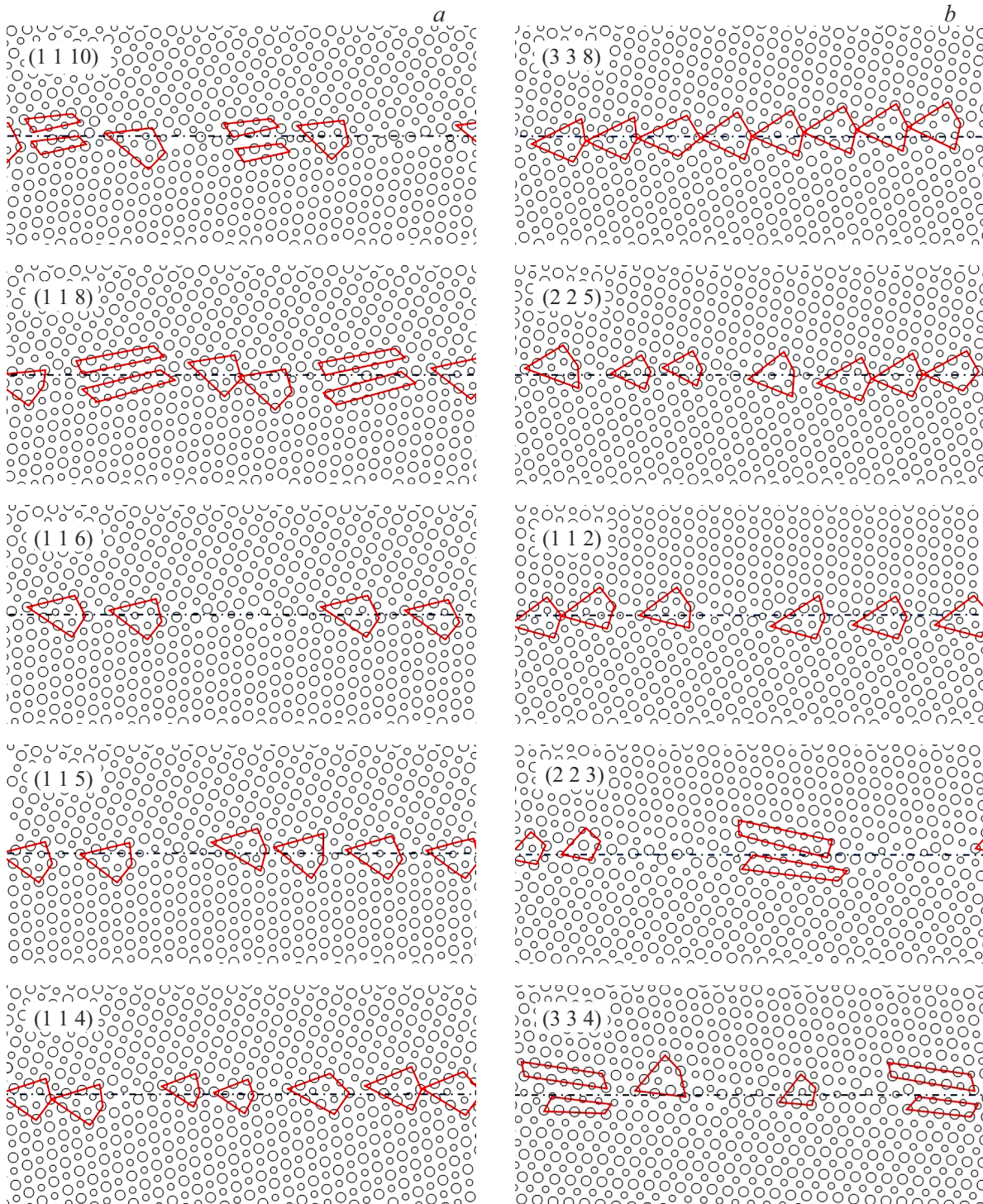


Figure 3. Structure of asymmetrical grain boundaries: a) $\Theta_1 < \Theta/2$; b) $\Theta_1 > \Theta/2$.

boundaries contain a small number of basic structural elements of the $\Sigma 3(112)$ boundary. The boundaries with widely different angles Θ_1 and Θ_2 feature structural areas where almost ideal crystals are adjacent. Boundaries (116) and (223) contain in their structures quite large segments that could not be described in terms of the structural unit model.

3. Procedure for examination of atom hopping isotropy

According to [22], three main grain-boundary self-diffusion mechanisms are defined: vacancy, pipe and atom migration on grain-boundary vacancies. In the vacancy mechanism, vacancies migrate over atom locations in the

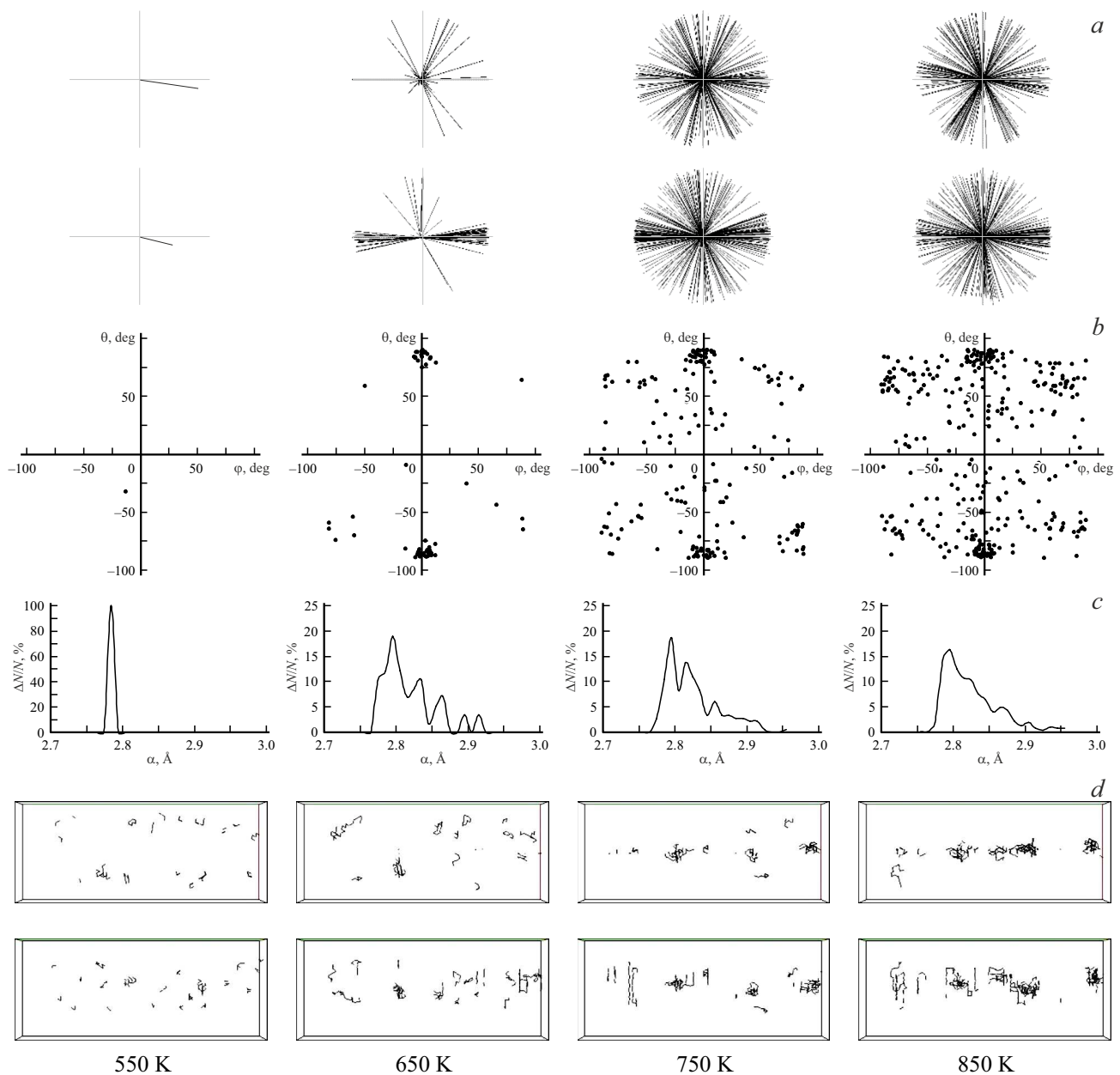


Figure 4. Temperature dependence of isotropy of self-diffusion on special GB $\Sigma 11(113)$: *a*) hedgehogs; *b*) isotropy charts; *c*) length of atomic hops; *d*) vacancy tracks.

structural unit. Hopping directions reflect atomic configuration of structural units. This mechanism is implemented in GB with low excessive volume and quite homogeneous distribution. Migration of atoms over grain-boundary vacancies that are formed due to GB restructuring during thermal motion of atoms is defined as atom walk from one structural unit to another. Formation of a grain-boundary vacancy may occur in any area of a structural unit, therefore hopping directions on the distributed vacancies are of random nature. Pipe mechanism is defined as the mechanism where atoms move over those GB that contain channels with a higher local free volume compared with the mean volume. self-diffusion mechanisms were determined by tracking the

individual atom motion. Hop direction and magnitude are shown as a segment connecting the start and end position of the atoms. To analyze the full range of atom motions, the study used the following technique: all atom hops in the defect area were tracked during some time period. Start and end atom positions were defined. Then, all segments were joined by their start position points as a result a three-dimensional figure was built that provided visualization of the isotropy of elementary atom hopping during diffusion. These figures were called hedgehogs [23]. Figure 4, *a* shows the projections of hedgehogs onto the plane perpendicular to the misorientation axis (upper projection) and the GB plane (lower projection) for special GB $\Sigma 11(113)$ at various

temperatures. Though the hedgehogs are suitable for visualization of hopping isotropy, they are still insufficient for analysis. For the analysis, we used pictures called isotropy charts that were built as follows. In the spherical coordinate system, the hopping direction is specified by angle φ measured from the misorientation axis in the GB plane and angle θ measured from the direction of the perpendicular to the boundary plane. Each hop was marked by a point on the plane with its coordinates being angles φ (horizontal axis) and θ (vertical axis). Hopping isotropy charts for boundary $\Sigma 11(113)$ are shown in Figure 4, *b*. If a point falls into a region with coordinates φ close to zero, then the corresponding hopping direction is aligned with the boundary misorientation axis; if this angle is close to $\pi/2$, the hopping direction is perpendicular to it. If angle θ is close to zero, hopping proceeds in the direction perpendicular to the plane of the boundary; if this angle is close to $\pi/2$, the hopping direction lies within the GB plane.

It follows from the figure that hopping is strongly anisotropic at low temperatures (550 K and 650 K). The greatest number of hops corresponds to angles $\varphi \approx 0^\circ$ and $\theta \approx 90^\circ$, which characterize hops in the boundary plane along the misorientation axis. This is due to the structure of the boundary, which consists of short structural elements and has no channels for unhindered motion of atoms. The chaotic component becomes more and more apparent as the temperature increases. While there are much fewer hops at an angle to the misorientation axis than along it at a temperature of 650 K, such hops become dominant already at 750 K, indicating a change in the diffusion mechanism. Atom hop length α allows one to estimate the fraction of atomic displacements via the vacancy mechanism. With the vacancy mechanism, the hop length is equal to the interatomic distance. Figure 4, *c* shows the distributions of the number of hops (expressed as a percentage) with their length at different temperatures. It can be seen that the fraction of hops corresponding to the interatomic distance decreases with increasing temperature, while the fraction of longer hops increases significantly. This is also indicative of a significant contribution of hopping via the mechanism of migration of atoms along grain boundary vacancies.

In the process of self-diffusion via the vacancy mechanism, atoms shift sequentially over one interatomic distance. A vacancy causing this series of hops may move over long distances. The entire set of hops occurring within a certain time interval at a certain temperature produces a three-dimensional pattern of the trajectories of vacancies, which was projected onto a plane perpendicular to the GB misorientation axis (upper projection) and onto the boundary plane (lower projection) at different temperatures (Figure 4, *d*). At low temperatures, the motion of atoms is of a pronounced vacancy nature, and almost no hops in the boundary are observed. As the temperature rises, the percentage of hops in the boundary increases (with atoms moving predominantly along the misorientation axis). At even higher temperatures, almost all hops lie in the boundary plane, but a significant number of chaotic shifts of atoms are observed along with diffusion along the misorientation axis.

4. Isotropy of hops of atoms of asymmetric grain boundaries

The results of analysis of hedgehogs and anisotropy charts for asymmetrical GBs revealed that a preferred direction of hops along the misorientation axis is retained at all temperatures. However, as the temperature rises, hops acquire a significant chaotic component. Having analyzed isotropy charts, we found no hops with angle $\varphi = 0^\circ$ at any temperature; thus, atoms do not move perpendicular to the GB plane. At the lowest temperature, several boundaries (namely, (1110), (118), and (112)) do not have clearly defined hopping directions. However, as the temperature rises, the percentage of hops along the misorientation axis becomes more and more significant. The chaotic component in the orientation of hops becomes significantly more pronounced for all boundaries within the 650–750 K temperature range. At high temperatures (approximately 900 K), atoms hop in almost any direction along the GB, although the greatest number of hops are still aligned with the misorientation axis.

A complete picture of isotropy of atomic motion may be obtained by analyzing hedgehogs, isotropy charts, and vacancy tracks simultaneously. The study of tracks revealed that hops occur in local areas of the boundary at low temperatures. The hopping intensity depends on the crystal geometry of the boundary and the degree of deformation of structural elements. Specifically, angles Θ_1 and Θ_2 for two boundaries (1110) and (334) differ widely, and severely deformed structural elements are thus present in their structure. At the same time, the boundaries have regions that could be characterized within the model of structural units. As a consequence, the diffusion motion is uniform over the entire boundary plane (with the most intense diffusion proceeding along highly deformed regions of the boundary). This is illustrated by Figure 5, *a*, which shows boundary (0110) with diffusion motion superimposed on it. In contrast, boundary (338) has many almost ideal structural elements; therefore, large sections of this GB are not subject to the diffusion motion of atoms (Figure 5, *b*).

As the temperature rises, the intensity of atomic hopping and the width of the diffusion zone increase. In addition, as was demonstrated in [24], lattice vacancies sink to the boundary in the process of diffusion motion. At high temperatures, the diffusion zone has a width on the order of two lattice parameters, and hopping proceeds along almost the entire length of the boundary. Analysis revealed that regions with a highly deformed structure, where the motion of atoms is the most intense, form in the structure of boundaries during heating. Thus, the self-diffusion mechanism changes in asymmetrical GBs as well. However, owing to the irregular structure of such boundaries, these changes are not as well-pronounced as those in special GBs.

As was noted above, boundaries (116) and (223) contain fairly large structural sections that could not be characterized within the structural unit model. These sections are also sections of the boundary with accelerated diffusion even at low temperatures (Figure 5, *c*).

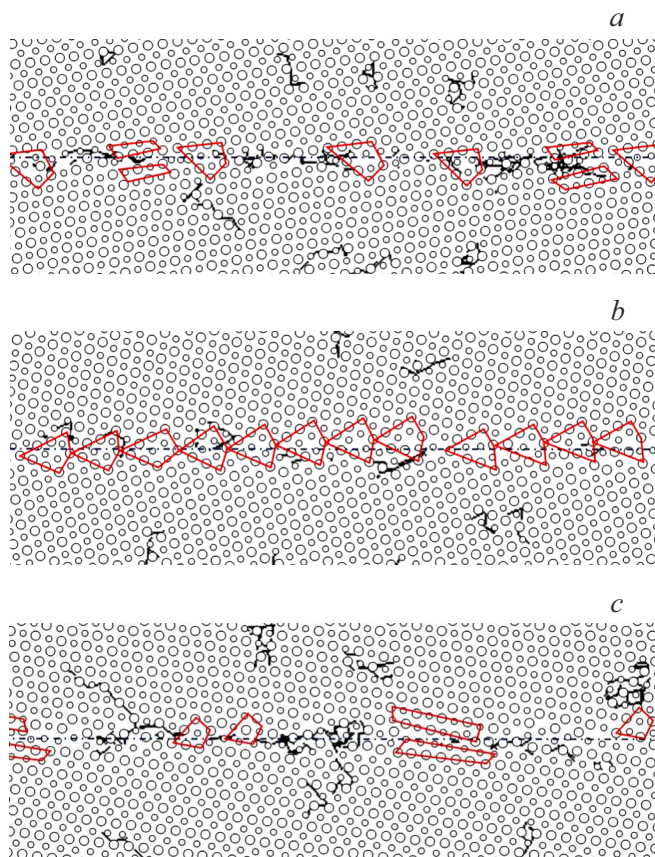


Figure 5. Diagrams of atomic hops with structural elements superimposed on them: *a*) (1110); *b*) (338); *c*) (223).

5. Grain-boundary diffusion parameters

As follows from Figure 4, *c*, during diffusion on GB hopping distance is close to the radius of the first coordination sphere because the boundary structure retains the short-range order. Interatomic distances in the boundary region may decrease or increase by several percent that does not exceed common errors of experimental determinations of diffusion constant. Therefore, the assumption of a single hopping distance equal to the radius of the first coordination sphere is permissible for the investigation of diffusion mechanisms in areas with excessive and confined free volume. However, the diffusion activation energy in the GB region may decrease considerably. The self-diffusion parameters were found herein from observations over atom motions during heating of a crystal containing the boundary. Self-diffusion coefficients were determined based on the number of atom hops (Γ) in accordance with the following expression: $D_{GB} = \frac{1}{6} \alpha^2 \Gamma = \frac{1}{12} a^2 \Gamma$ [25], where $\alpha = r_1 = a\sqrt{2}/2$ is the unit distance of atom hopping. Figure 6, *a* shows the results of calculation of diffusion constants for GB $\Sigma 11(113)$ with the use of different potentials. The figure shows that the diffusion constants have close values. Moreover, two linear segments are clearly seen on the curve, and therefore the diffusion mechanism

changes at a certain temperature. As shown in [26], variation of the Arrhenius curve slope is associated with restructuring of this boundary.

Figure 6, *b* shows dependences of diffusion constants for asymmetrical GB on temperature. Each point is an averaged diffusion constant calculated using the Morse and Cleri–Rosato potentials. For convenience, these dependences are spread over the vertical axis because the diffusion constants have close values. For boundaries with $\Theta_1 < \Theta/2$, the values of the logarithm of diffusion constants are increased; for $\Theta_1 > \Theta/2$, they are reduced by adding ± 0.5 , ± 1.0 , ± 1.5 , etc. The dependence for a symmetric GB $\Sigma 11(113)$ with unchanged diffusion constants is shown for comparison in the figure.

High-temperature ($1/T < 1.25 \cdot 10^{-3} \text{ K}^{-1}$) and low-temperature ($1/T > 1.25 \cdot 10^{-3} \text{ K}^{-1}$) regions may be distinguished in these dependences. The slopes of dependences are almost the same for all boundaries in the high-temperature region. This is attributable to the fact that the structure of boundaries loses its distinct character at high temperatures due to the high mobility of atoms. In the low-temperature region, the dependences have 1–2 linear segments. The difference in slopes of plots may be interpreted as a change in the predominant mechanism of grain-boundary diffusion (associated with restructuring of the boundary) upon heating. The slope of dependences increases with increasing temperature for the majority

Table 2. Parameters of grain-boundary self-diffusion in the low-temperature region: activation energy (in kJ/mol and eV) and pre-exponential factor (cm^2/s)

GB	Q , kJ/mol	Q , eV	D_0 , cm^2/s
$\Theta_1 < \Theta/2$			
1110	26.9	0.277	$4.89 \cdot 10^{-09}$
118	12.1	0.125	$3.78 \cdot 10^{-10}$
	41.6	0.429	$5.69 \cdot 10^{-7}$
116	23.0	0.237	$1.92 \cdot 10^{-09}$
	9.2	0.095	$1.48 \cdot 10^{-10}$
115	13.2	0.136	$3.98 \cdot 10^{-10}$
114	20.9	0.216	$1.64 \cdot 10^{-09}$
$\Theta_1 > \Theta/2$			
338	29.5	0.304	$9.24 \cdot 10^{-09}$
	10.5	0.109	$1.86 \cdot 10^{-10}$
225	14.7	0.151	$6.47 \cdot 10^{-10}$
	8.5	0.088	$1.27 \cdot 10^{-10}$
112	26.8	0.276	$4.72 \cdot 10^{-09}$
223	39.3	0.405	$4.28 \cdot 10^{-08}$
	20.6	0.212	$1.69 \cdot 10^{-09}$
334	33.1	0.393	$3.61 \cdot 10^{-08}$
	9.6	0.099	$2.11 \cdot 10^{-10}$

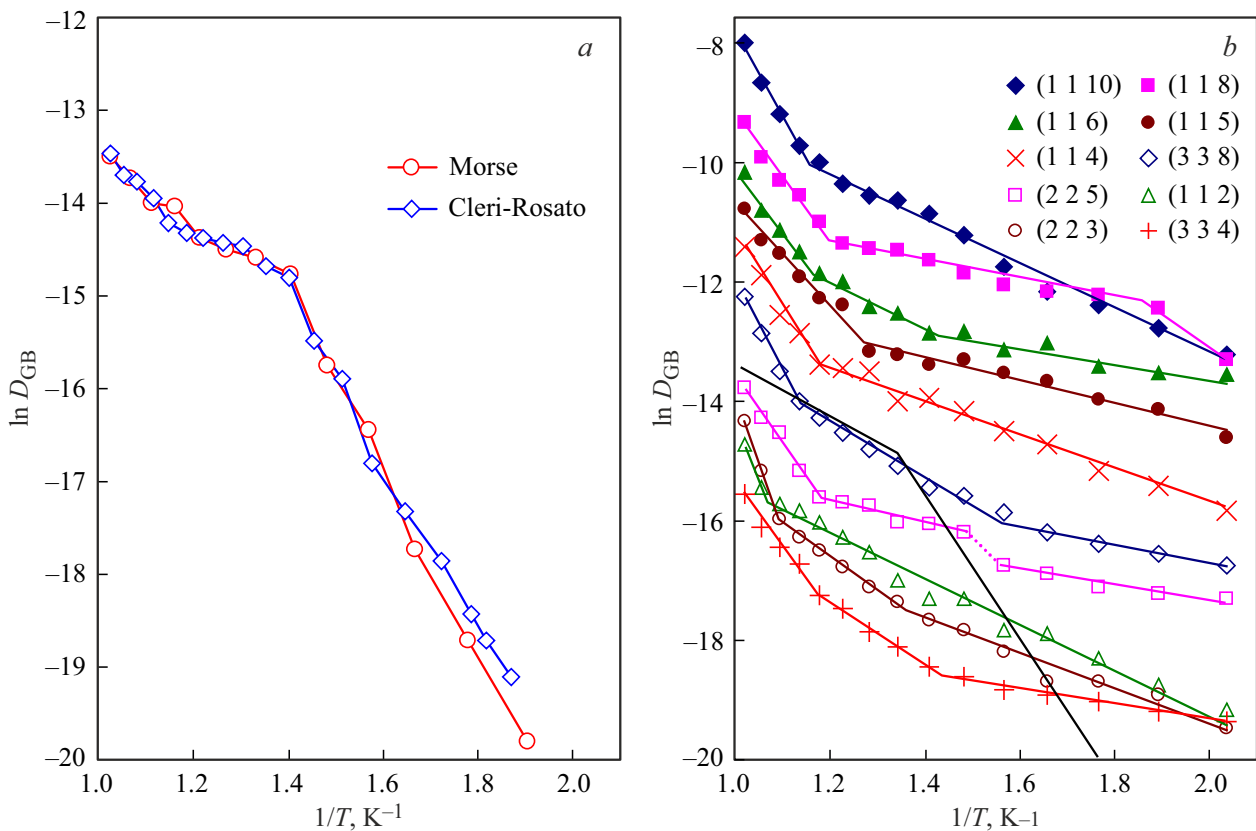


Figure 6. Temperature dependences $\ln D_{GB}$: a) special GB $\Sigma 11(113)$; b) asymmetrical GBs.

of boundaries. The exception is boundary (118): the slope of the corresponding dependence decreases at higher temperatures.

Parameters of the Arrhenius dependences of grain-boundary self-diffusion in the low-temperature region were determined from the plots. The values of self-diffusion parameters D_0 and Q are listed in Table 2. The growth of activation energy with increasing temperature is apparently associated with the transformation of structural elements of boundaries and an increased contribution of atomic hopping along grain-boundary vacancies. The exception is boundary (118): the activation energy corresponding to it decreases. The structure of this boundary features large areas where almost ideal crystals are adjacent and form interfaces of different crystallographic planes with hindered diffusion along them. As the temperature increases, the structures get deformed, thus facilitating diffusion.

6. Melting of asymmetric grain boundaries

High-temperature regions of grain-boundary diffusion are characterized by almost identical slopes of the Arrhenius dependence, but cover different temperature intervals. Specifically, this section starts at temperatures ~ 750 K for GB (115); at temperatures higher than 900 K for bound-

aries (112) and (223); and at different temperatures around 800 K for the other boundaries. This gives reason to believe that GB melting also occurs at different temperatures. A technique for determining the melting temperature of a GB was developed in [27], and it was demonstrated that boundaries may melt at temperatures both below and above the melting point of a single crystal. In the present study, the molecular dynamics experiment was extended to temperatures at which the bicrystal containing a boundary lost its crystallinity completely (i.e., went into a molten state). For comparison, we conducted an experiment on melting a single crystal with an equilibrium number of vacancies in accordance with the procedure detailed in [27] using both Morse and Cleri-Rosato potentials.

Calculations revealed that boundaries melt at various temperatures below the melting point of the single crystal. Data on these temperatures are listed in Table 3.

The values of GB melting temperature T_{GB} are presented relative to melting point T_m of a single crystal with an equilibrium number of vacancies. Boundaries (118), (338), and (112) have the highest melting points. Boundary (118) has large regions with a regular atomic structure, and the diffusion activation energy for this boundary (Table 2) is the highest among all the studied GBs. Boundary (338) is formed by structural elements that are closely adjacent to each other and lie near the GB plane. In addition,

Table 3. Melting temperature of asymmetrical GBs (T_{GB}/T_m), region of nucleation of the liquid phase, and width of the melted zone

GB	Morse			Clari–Rosato		
	T_{GB}/T_m	Region of nucleation of the liquid phase	Width of the melted zone	T_{GB}/T_m	Region of nucleation of the liquid phase	Width of the melted zone
$\Theta_1 < \Theta/2$						
(1110)	0.951	<i>top</i>	<i>low</i>	0.962	<i>top</i>	<i>low</i>
(118)	0.977	<i>centre</i>	<i>middle</i>	0.968	<i>top</i>	<i>high</i>
(116)	0.946	<i>top</i>	<i>low</i>	0.949	<i>centre</i>	<i>middle</i>
(115)	0.954	<i>centre</i>	<i>high</i>	0.943	<i>top</i>	<i>middle</i>
(114)	0.960	<i>top</i>	<i>middle</i>	0.956	<i>centre</i>	<i>middle</i>
$\Theta_1 > \Theta/2$						
(338)	0.960	<i>centre</i>	<i>high</i>	0.987	<i>centre</i>	<i>high</i>
(225)	0.948	<i>centre</i>	<i>high</i>	0.955	<i>bottom</i>	<i>middle</i>
(112)	0.963	<i>centre</i>	<i>high</i>	0.968	<i>centre</i>	<i>high</i>
(223)	0.931	<i>bottom</i>	<i>low</i>	0.917	<i>bottom</i>	<i>low</i>
(334)	0.937	<i>bottom</i>	<i>middle</i>	0.911	<i>bottom</i>	<i>low</i>

angles Θ_1 and Θ_2 are similar; therefore, the structural elements in this boundary are the least deformed. This is the reason why the diffusion motion of atoms in the region of this boundary is insignificant (Figure 5, *b*). A similar pattern is observed for the (112) boundary that contains fairly regular structural elements located at equal distances from each other and has an Arrhenius dependence with one linear section. Boundaries (223) and (334) have the lowest temperatures. They consist of the most deformed structural elements and contain large regions that could not be characterized within the model of structural units. The diffusion of atoms in these regions is the most intense (Figure 5, *c*), affecting the temperature of disordering of the grain-boundary layer. The melting temperature of the remaining boundaries averages at $0.95T_m$.

Data on the regions of nucleation of the liquid phase and the width of the molten layer are also presented in Table 3. Grains with angles Θ_1 and Θ_2 are denoted as „*top*“ and „*bottom*“, respectively. The „*center*“ region represents nucleation of the liquid phase in the boundary plane. The „*low*“, „*middle*“, and „*high*“ melted zone widths correspond to the following numbers of lattice parameters: less than 2, 2–4, and more than 4, respectively.

7. Conclusion

The study investigated grain-boundary self-diffusion on asymmetrical grain boundaries with misorientation axis [110]. Self-diffusion behavior and boundary structure were compared. High-temperature grain-boundary diffusion processes were examined. The following conclusions are made.

1. All the studied asymmetrical boundaries consist of the same structural elements as special boundary $\Sigma 11(113)$,

which are strained and rotated about the boundary plane. The distance between the elements varies from zero to 1.5 lattice parameters. Half of the boundaries have areas where grains are joined almost without lattice distortion. For some boundaries, there are segments that could not be described in terms of the structural unit model.

2. Atom hopping in projection onto the plane perpendicular to the misorientation axis reveals anisotropy of hopping for all temperatures. As the temperature rises, hops acquire a significant chaotic component. In the projection on the GB plane, the hopping anisotropy is much less pronounced. Diffusion is more active on those GB whose structural elements are most strained. The boundary segments that could not be described in terms of the structural unit model are also the segments with accelerated diffusion.

3. The Arrhenius dependences were plotted to determine the grain-boundary diffusion parameters. High-temperature and low-temperature regions may be identified on the dependences. All curves have the same slopes in the high-temperature region because boundaries lose their structural identity at high temperature. In the low-temperature region, the curves have from one to two linear segments. Slope variation may be interpreted as switch of the preferred self-diffusion mechanism.

4. Melting on the grain boundaries was studied. At high temperatures, the grain-boundary region is amorphized earlier than the adjacent grains. This suggests that the boundaries melt at lower temperatures than were from 0.91 to 0.98 of the melting temperature of a single-crystal with equilibrium number of vacancies.

Conflict of interest

The authors declare that they have no conflict of interest.

References

- [1] W. Seith Diffusion in metallen: Platzwechselreaktionen. Springer-Verlag. (1955). 306 p.
- [2] A. Suzuki, Y. Mishin. *Interface Sci.* **11**, *1*, 131 (2003)
- [3] A. Suzuki, Y. Mishin. *J. Mater. Sci.* **40**, *12*, 3155 (2005).
- [4] T. Frolov, Y. Mishin. *Phys. Rev. B* **79**, *17*, 174110 (2009).
- [5] T. Frolov, D.L. Olmsted, M. Asta, Y. Mishin. *Nature Commun.* **4**, 1899 (2013).
- [6] E.G. Kharina, M.D. Starostenkov, G.M. Poletaev, R.Yu. Rakitin. *Phys. Solid State* **53**, *5*, 1043 (2011).
- [7] R. Mohammadzadeh, M. Mohammadzadeh. *J. Appl. Phys.* **124**, *3*, 035102 (2018).
- [8] I.I. Novoselov, A.Yu. Kuksin, A.V. Yanilkin. *Phys. Solid State* **56**, *5*, 1025 (2014).
- [9] S. Yang, S.-H. Yun, T. Oda. *Fusion Eng. Des.* **131**, *105* (2018).
- [10] M.I. Mendeleev, H. Zhang, D.J. Srolovitz. *J. Mater. Res.* **20**, *5*, 1146 (2005).
- [11] J.D. Rittner, D.N. Seidman. *Phys. Rev. B* **54**, *10*, 6999 (1996).
- [12] E.R. Homer, S.M. Foiles, E.A. Holm, D.L. Olmsted. *Acta Mater.* **61**, *4*, 1048 (2013).
- [13] A.V. Weckman, A.S. Dragunov, B.F. Dem'yanov, N.V. Adarich. *Russ. Phys. J.* **55**, *7*, 799 (2012).
- [14] P.M. Morse. *Phys. Rev.* **34**, *1*, 57 (1929).
- [15] F. Cleri, V. Rosato. *Phys. Rev. B* **48**, *1*, 22 (1993).
- [16] A.I. Tsaregorodtsev, N.V. Gorlov, B.F. Dem'yanov, M.D. Starostenkov. *Phys. Met. Metallogr.* **58**, *2*, 336 (1984).
- [17] A.V. Weckman, B.F. Dem'yanov. *Phys. Solid State* **63**, *1*, 54 (2021).
- [18] A.V. Weckman, B.F. Dem'yanov. *Phys. Met. Metallogr.* **120**, *1*, 50 (2019).
- [19] M.D. Starostenkov, B.F. Dem'yanov, A.V. Vekman. *Surface Investigation: X-Ray, Synchrotron and Neutron Techniques* **16**, *4*, 645 (2001).
- [20] A.V. Vekman, B.F. Dem'yanov, M.D. Starostenkov. *Steel Transl.* **31**, *2*, 54 (2001).
- [21] A.V. Weckman, B.F. Dem'yanov. *FPSM* **14**, *4*, 480 (2017). (in Russian).
- [22] B.F. Dem'yanov, A.S. Dragunov, A.V. Weckman. *Izv. Altai State Univ. 1–2* (65). 158 (2010). (in Russian).
- [23] A.S. Dragunov. *Extended Abstract of Cand. Sci. Dissertation, Barnaul* (2012). 23 s. (in Russian).
- [24] A.V. Weckman, B.F. Dem'yanov, A.S. Dragunov. *Phys. Met. Metallogr.* **116**, *6*, 586 (2015).
- [25] B.S. Bokshstein. *Atomy bluzhdayut po kristallu*. Nauka, M. (1984). 208 s. (in Russian).
- [26] A.V. Weckman, B.F. Dem'yanov, I.A. Shmakov. *Izv. Altai State Univ. 1–2* (77), 141 (2013). (in Russian).
- [27] A.V. Weckman, B.F. Dem'yanov, A.S. Dragunov. *Russ. Phys. J.* **58**, *12*, 1732 (2016).

Translated by E.Ilinskaya